CORONAVIRUS

# Ultrafast, sensitive, and portable detection of COVID-19 IgG using flexible organic electrochemical transistors

**Hong Liu[1], Anneng Yang[1], Jiajun Song[1], Naixiang Wang[1], Puiyiu Lam[1], Yuenling Li[1], Helen Ka-wai Law[2], Feng Yan[1]***



**The outbreak of COVID-19 and its continued spread have seriously threatened public health. Antibody testing is essential for infection diagnosis, seroepidemiological analysis, and vaccine evaluation. However, convenient, fast, and accurate antibody detection remains a challenge in this protracted battle. Here, we report an ultrafast, low-cost, label-free, and portable SARS-CoV-2 immunoglobulin G (IgG) detection platform based on organic electrochemical transistors (OECTs), which can be remotely controlled by a mobile phone. To enable faster detection, voltage pulses are applied on the gate electrode of the OECT to accelerate binding between the antibody and antigen. By optimizing ion concentrations and pH values of test solutions, we realize specific detection of SARS-CoV-2 IgG in several minutes with a detectable region from 10 fM to 100 nM, which encompasses the range of serum SARS-CoV-2 IgG levels in humans. These portable sensors show promise for use in diagnosis and prognosis of COVID-19.**

## INTRODUCTION

Coronavirus disease 2019 (COVID-19) caused by severe acute respiratory syndrome coronavirus 2 (SARS-CoV-2) has been spreading globally since January 2020 (*1*). Although massive efforts have been undertaken in the past 1 year, the spread of the virus remains severe in many countries. The COVID-19 has not only posed a great threat to global public health but also caused enormous economic and social burdens on affected countries. Notably, rapid and accurate diagnosis of novel coronavirus infection plays an important role in choice of appropriate treatment methods, saving human lives, and preventing virus transmission. At present, novel coronavirus diagnosis is mainly divided into RNA detection and antigen antibody detection (*2*). Antibody testing plays an important role in the following aspects (*3*). First, it can be used to screen asymptomatic and RNA false-negative infections (*4*, *5*). Second, it is useful in clinical health assessment (*6*). Antibodies play a key role in neutralizing the virus. People with low antibody levels have a risk of secondary infection, and severely ill patients with low levels of antibodies may be at risk of death. Third, testing resultant antibodies is important for vaccine development and evaluation (*7*). Fourth, it is also important for seroepidemiological study for analyzing the infection rate and population immunity rate in different areas (*8*, *9*).

At present, COVID-19 antibodies are detected mainly by enzyme-linked immunosorbent assay (ELISA) (*10*) and colloidal gold lateral flow immunoassays (LFIAs) (*11*). ELISA is highly accurate, but the technical procedure is complicated, making it difficult to achieve both portable and high-throughput detection. LFIA is easy to operate and portable, but with relatively low sensitivity and prone to misdiagnosis. Therefore, for the detection of COVID-19 antibody, we need to develop a highly sensitive and rapid detection method that can be easily operated for point-of-care testing and screening of large populations. In addition to serum-based assays, SARS-CoV-2 immunoglobulin G (IgG) can be detected in saliva, with the advantages of a noninvasive process and the possibility of self-collection of samples. Because antibody concentration in human saliva is several orders of magnitude lower than in serum, high analytical sensitivity is needed (*12*–*14*).

Organic electrochemical transistors (OECTs) have been recognized as high-performance transducers and amplifiers that can convert biological signals into electrical signals. OECT-based biosensors have the advantages of high sensitivity, low cost, easy fabrication, and mechanical flexibility and are suitable for high-throughput and multiplexing detections of biomarkers (*15*–*17*). A typical OECT has a simple device structure that consists of three electrodes (gate, source, and drain), an organic semiconductor channel between source and drain, and an electrolyte medium connecting the gate and the channel. The device has a low working voltage, good biocompatibility, and excellent stability in the electrolyte (*18*). In recent years, OECTs have been successfully used in the detection of various biomolecules, including nucleic acids, proteins, and metabolite (*19*–*22*). Here, we report OECT-based biosensors for the detection of SARS-CoV-2 IgG, which is controlled by a portable meter and a mobile phone through Bluetooth. SARS-CoV-2 spike protein is immobilized on the gate electrode through covalent binding, and SARS-CoV-2 IgG is bound with spike protein through antibody-antigen reaction during incubation, leading to a response of the device performance. Our device can detect SARS-CoV-2 IgG with an ultralow detection limit of 1 fM in aqueous solutions and 10 fM in serum and saliva. The detection range in serum is from 10 fM to 100 nM with a good linear relationship, perfectly matching the serum-specific IgG levels in patients with COVID-19. The ultralow detection limit in saliva can also satisfy the needs of exquisite analytical sensitivity (*12*, *13*). To accelerate the testing process, we developed a novel technique by applying voltage pulses on the gate during incubation, which can decrease the incubation time of about 50%. Because of the rapid reaction of antigens and antibodies and the label-free approach, the whole test time can

[1]Department of Applied Physics, The Hong Kong Polytechnic University, Hung Hom, 999077 Kowloon, Hong Kong. [2]Department of Health Technology and Informatics Faculty of Health and Social Sciences, The Hong Kong Polytechnic University, Hung Hom, 999077 Kowloon, Hong Kong.
*Corresponding author. Email: apafyan@polyu.edu.hk

be completed within 5 min. Excellent selectivity of the devices for SARS-CoV-2 IgG detection is verified in our results.

## RESULTS

### Design of the device and portable measurement system

OECTs are fabricated on a plastic PET substrate by photolithography (fig. S1) in which Au source, drain, and gate electrodes are deposited by magnetron sputtering and an organic channel made of poly(3,4-ethylenedioxythiophene)–poly(styrenesulfonate) (PEDOT:PSS) is prepared by spin coating (*23*). The patterned PEDOT:PSS channel (fig. S1L) is between the source and drain electrodes, and an insulating layer (SU8 photoresist) is in the left area for electrode encapsulation. The device is connected to a portable meter (Fig. 1) that is controlled by a mobile phone through Bluetooth. The device performance is measured by dripping a small volume (5 μl) of aqueous solution [e.g., phosphate-buffered saline (PBS) solution] on the surface. Under optimum fabrication conditions, the device shows very stable performance in PBS solution and a fast response of channel current to a change of gate voltage (fig. S2).

The Au gate can be conveniently modified with biomolecules on the surface and used for sensing SARS-CoV-2 IgG (Fig. 1). The clean Au electrode is first modified with a chemical self-assembled monolayer (SAM) of mercaptoacetic acid (MAA) through gold-thiol binding (*24*). After the chemical activation of the carboxylic groups, the antigen (SARS-CoV-2 spike protein) is conjugated to the chem-SAM layer through the covalent bond between carboxyl and amino group. Bovine serum albumin (BSA) is added afterward to fill the vacancy left and minimize nonspecific bindings. Subsequently, 5 μl of solution of target SARS-CoV-2 IgG is incubated on the gate electrode for a certain period of time (≤30 min). The receptor binding domain (RBD) of spike protein can specifically bind with SARS-CoV-2 IgG. The device is rinsed by deionized (DI) water after each step. Last, the device is measured by the meter after dripping 5 μl of electrolyte on the device surface. SARS-CoV-2 IgG solutions with different concentrations are tested with the OECT sensors to obtain the relationship between the device response and the IgG concentration.

Atomic force microscopy (AFM) was used to confirm effective antigen and antibody immobilization on the gate electrode (fig. S3). The stepwise modification images were presented with different image color bars for better observation (fig. S3, A and B). The Gaussian fits to the height histograms (fig. S3C) can visualize the gradual increase in height. Before the immobilization of spike protein, the gold gate electrode exhibits a smooth surface, and the root mean square (RMS) roughness is 0.32 nm. The height of the Au grains on the gate electrode is 1.87 ± 0.66 nm. After the immobilization of spike protein, massive particles can be observed on the surface of the gold electrode. The average size of the spike protein is 10 to 20 nm, and the feature height of particles after BSA blocking is 4.59 ± 1.75 nm. The RMS roughness is increased to 0.798 nm. Furthermore, with the binding of SARS-CoV-2 IgG to spike protein, a notable increase in particle size can be observed. The particle radius is 20 to 30 nm, and the RMS roughness is further increased to 0.885 nm. The height of protein particles is increased to 8.17 ± 1.77 nm, verifying the binding of antibody with antigen. The height of antigen and antibody complex is around 6.3 nm, which is similar with those previously reported (*25*, *26*). The successful immobilization of protein on the gate surface is also confirmed by Fourier transform infrared (FTIR) spectroscopy (fig. S4). Two prominent vibrational bands of the protein backbone can be observed after the immobilization of antigen and antibody (*27*, *28*).

### SARS-CoV-2 IgG detection

The detection process of IgG includes the following three steps: (i) to incubate a IgG solution on the gate modified with spike protein

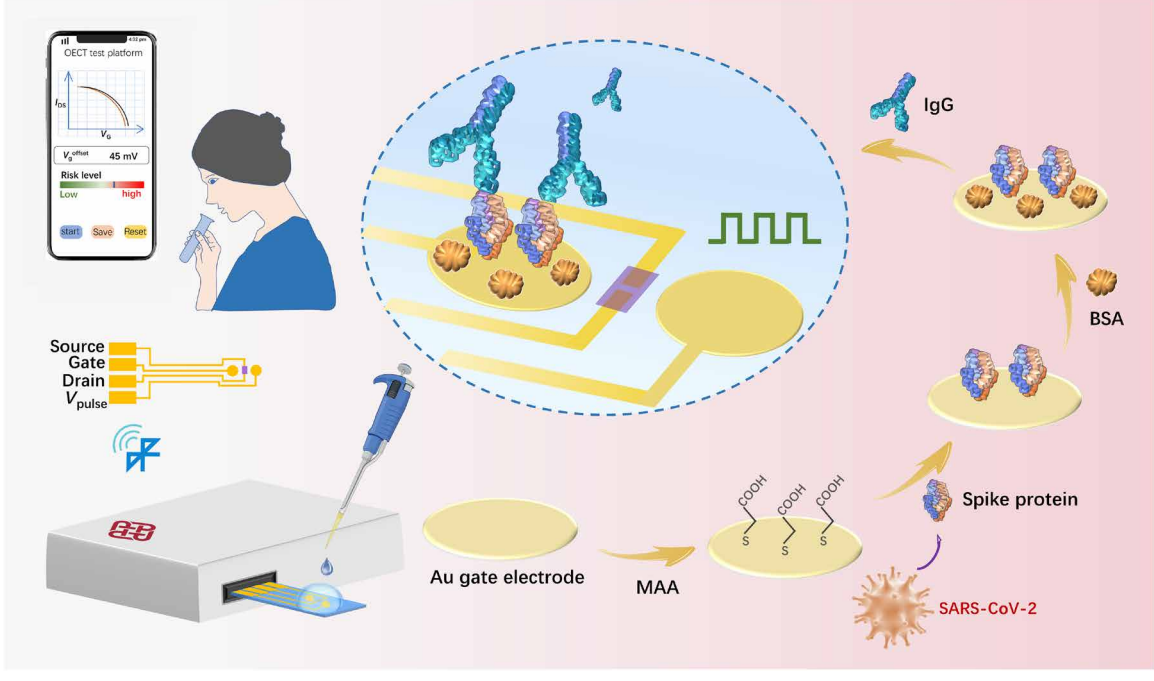


**Fig. 1. Scheme of the portable sensing system and the gate modification processes of the IgG sensor.** The device is connected to a portable meter that is controlled by a mobile phone through Bluetooth. The biological modification on a gate electrode is carried out with several steps.

for a certain period of time, (ii) to remove IgG solution and physically absorbed biomolecules on the gate by rinsing DI water, and (iii) to characterize the device performance in a separate electrolyte (see movie S1). The electrolyte properties such as the ion concentration and pH values can be optimized to get the biggest device response. Transfer curves ($I_{DS}$ versus $V_G$) of OECTs are tested before and after the immobilization of SARS-CoV-2 IgG (Fig. 2A). At the beginning, the electrolyte used for testing is 10 mM PBS solution with a pH value of 7.2, which is regarded as the commonly used test environment. With the increase of SARS-CoV-2 IgG concentration, the transfer curves gradually shift toward more negative gate voltages. The inset is the enlarged graph of the transfer curves. Seventy-two–millivolt gate voltage shift $\Delta V_G$ is observed with 100 nM SARS-CoV-2 IgG incubated on the gate electrode for 10 min. The detection limit is 10 pM, corresponding to a gate voltage shift $\Delta V_G$ of 12 mV (Fig. 2B). The voltage shift can meet the requirement of signal-to-noise (S/N) ratio higher than 3 for the detection limit (*29*). All tests were repeated at least three times.

Proteins are made up of zwitterionic amino acid compounds, which can be positively or negatively charged depending on the isoelectric point (pI) and pH value of the electrolyte (*30*). The SARS-CoV-2 IgG is positively charged in PBS solution (pH 7.2) because its pI is calculated to be 8.2 by online bioinformatics resource Expasy. The surface potential of the gate electrode can be influenced by charged molecules and change the effective gate voltage of the transistor. The positive charge of protein induces an electric dipole and a potential barrier across the electric double layer (EDL) on the gate/electrolyte interface (Fig. 2C).

The channel current $I_{DS}$ of an OECT is given by the following equations (*31*, *32*)

$$I_{DS} = \frac{W\mu C_i}{L}\left(V_P - V_g^{eff} + \frac{V_{DS}}{2}\right)V_{DS} \ (\text{when} \ |V_{DS}| \ll |V_p - V_g^{eff}|)$$
$$V_P = qp_0 t/C_i$$
$$V_g^{eff} = V_G + V_{offset} \quad (1)$$

where $W$ is the channel width, $L$ is the channel length, μ is the hole mobility, $C_i$ is the effective capacitance per unit area of the transistor, $V_p$ is the pinch-off voltage, $V_g^{eff}$ is the effective gate voltage, $q$ is electronic charge, $p_0$ is the initial hole density in the organic semiconductor before the application of a gate voltage, $t$ is the thickness of the organic semiconductor film, and $V_{offset}$ is the offset voltage related to the potential drop at the two EDL interfaces (*33*). $C_i$ is equal to the total capacitance of the two interfacial capacitors connected in series, which is given by (*33*)

$$C_i = \frac{C_g C_d}{(C_g + C_d)S} \quad (2)$$

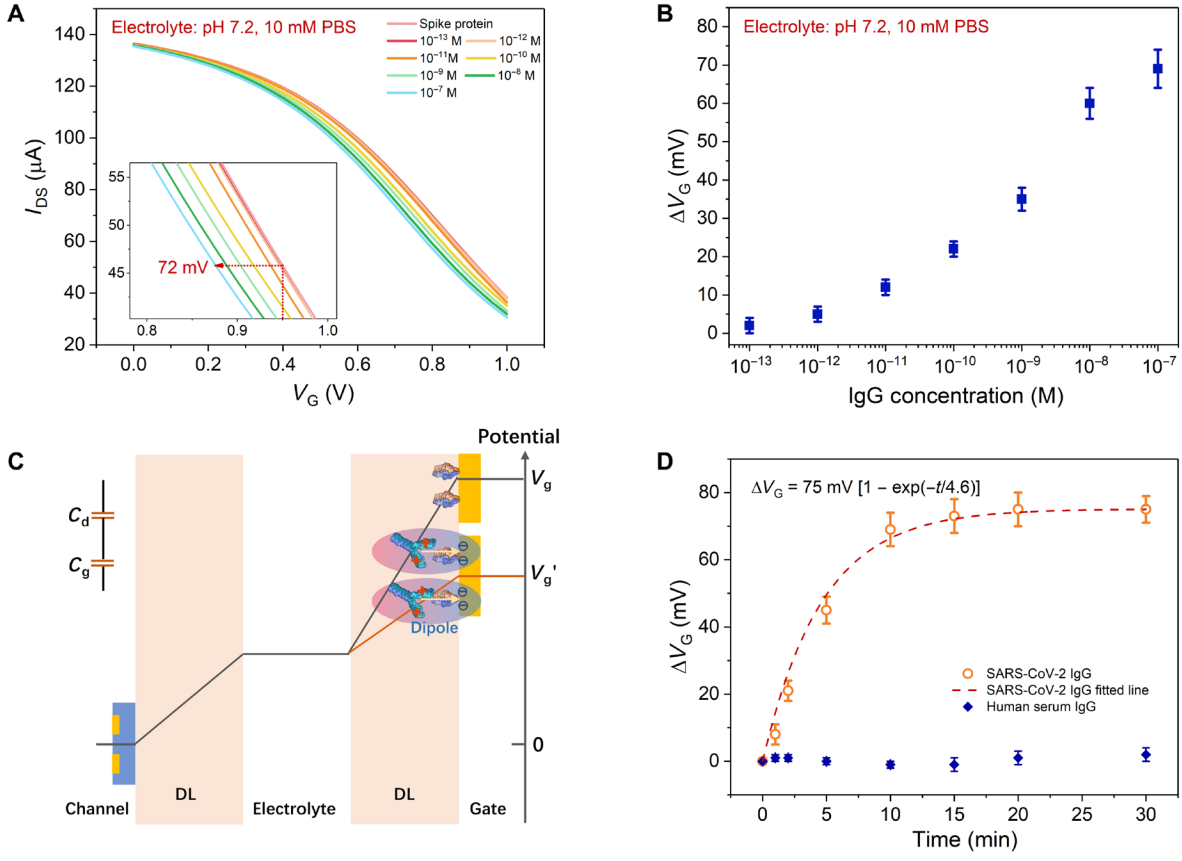


**Fig. 2. Detection of SARS-CoV-2 IgG using OECTs operated in PBS solution.** (**A**) The transfer characteristics of OECTs after incubation of SARS-CoV-2 IgG solutions with different concentrations in sequence. (**B**) Relative change of the gate voltage $\Delta V_G$ as a function of IgG concentration. (**C**) Schematic diagram for protein dipole and potential drops in the two double layers. The arrow in the dipole shows the electric field generated by the positive charge of protein on the gate surface. (**D**) Relative change of the gate voltage $\Delta V_G$ as a function of incubation time. (All tests were conducted in electrolyte: 10 mM PBS, pH 7.2.)

where $C_d$ and $C_g$ are the capacitances of the interfaces between the electrolyte and PEDOT:PSS and between the electrolyte and Au gate, respectively. $S$ is the area of active layer.

After the immobilization of SARS-CoV-2 IgG on the gate surface, an electric dipole is formed on the gate surface. The induced potential change on the Au gate electrode can be expressed by (*34*)

$$\Delta\varphi = \frac{nQ_{IgG}}{\varepsilon_0\varepsilon_r}t_{IgG} \quad (3)$$

where $n$ is the coverage of protein molecules on the surface of gate electrode, which is related to the concentration SARS-CoV-2 IgG; $Q_{IgG}$ is the net charge for one IgG molecule, which is related to the pH value of the test environment; $\varepsilon_0$ is the dielectric permittivity of the free space; $\varepsilon_r$ is the relative dielectric constant of IgG layer; and $t_{IgG}$ is the effective interaction thickness related to the Debye length in the electrolyte, which will be discussed later. Thus, the positively charged protein on the gate surface can change the surface potential of the Au gate, leading to a shift of the transfer curve to a lower gate voltage.

Immobilization of SARS-CoV-2 IgG on the gate electrode shows little effect on the capacitance of the gate electrode $C_g$ (fig. S5). The typical dielectric constant $\varepsilon_r$ of a protein is about 3 (*35*), and the total height of antigen and antibody ($d$) is around 6.3 nm (fig. S3). According to $C = \varepsilon_r\varepsilon_0/d$, the capacitance of protein layer is around 0.42 μF/cm$^2$ if the electrode is fully covered with the protein. However, the actual value of the gate capacitance is much higher than that of a pure protein layer, indicating that the gate capacitance is mainly determined by the EDL and SAM layer on the Au gate surface.

Rapid detection is very important in the diagnosis of COVID-19 for continuous large numbers of infections (*36*). Notably, the devices are label-free and can be measured very quickly with a portable meter; thus, the test time is mainly limited by the incubation time of IgG on the sensor. Hence, we tried to find the optimum incubation time in the following experiment. SARS-CoV-2 IgG solution with a concentration of 100 nM was dripped on the gate area for a certain period of time for incubation, and then, the transfer curve of the device was measured in 10 mM PBS. This process on the same device was repeated for several times, and the device performance as a function of accumulated incubation time was obtained (fig. S6). Therefore, we can obtain the correlation between the gate voltage shift $\Delta V_G$ of the device and the incubation periods (Fig. 2D). The offset of the transfer characteristic gradually increases, and a significant response can be found even after 2-min incubation. The relationship can be fitted with an exponential function $\Delta V_G = A[1 - \exp(-t/\tau)]$, where $\tau = 4.6$ min is a time constant and $A = 75$ mV is the saturation value of $\Delta V_G$. Notably, the response of the device can reach 89% of the maximum shift after 10-min incubation and saturate after 20 min.

To confirm the specificity of the sensor in detecting SARS-CoV-2 IgG, IgG purified from normal human serum was tested with the same condition (fig. S7). The transfer curve of the device shows negligible shift after incubation in the human serum IgG for 10 min, while an obvious shift induced by SARS-CoV-2 IgG can be found at the same measurement condition (fig. S7A). The incubation of the sensor in pure BSA solution did not lead to any response in its transfer curve, indicating an excellent stability of the device in the aqueous solutions. In addition, the device was tested in the normal human serum IgG solution with different incubation periods, and no obvious signal was observed in the whole region, indicating excellent selectivity of the device (Fig. 2D). Furthermore, different concentrations of SARS-CoV-2 IgG mixed with 100 nM human serum IgG were tested by the device (fig. S7B). The device response to the SARS-CoV-2 IgG was not influenced by the serum IgG, indicating that the device could selectively detect the target antibody without any interference from other antibodies from serum.

### Sensitivity enhancement by increasing Debye length

In an electrolyte, a positively charged protein is surrounded by anions due to electrostatic interaction, and its surface charge can be screened within the Debye length of the EDL (*37*). Therefore, a protein with a distance to the gate longer than the Debye length should have little influence on the gate potential. Consequently, the Debye length, which is related to the ion concentration of an electrolyte, will markedly influence the performance of our IgG sensor. The Debye length in an electrolyte solution is given by (*38*)

$$\lambda_D = \sqrt{\frac{\varepsilon kT}{2N_A q^2 I}} \quad (4)$$

where $\varepsilon$ is the absolute permittivity of the electrolyte, $k$ is the Boltzmann's constant, $T$ is the temperature, $N_A$ is the Avogadro's number, and $I$ is the ionic strength of the solution.

To test the effect of Debye length on the device performance, the PBS electrolyte was diluted at different concentrations (10 mM, 1 mM, 100 μM, 10 μM, and 1 μM) and used in the detections of SARS-CoV-2 IgG. The shifts of the transfer curves measured in 10 μM PBS (Fig. 3A) are more pronounced in comparison with the responses obtained in 10 mM PBS solution. Notably, the maximum gate voltage offset $\Delta V_G$ corresponding to 100 nM IgG is increased from 72 to 127 mV. Figure 3B shows the shifts of the transfer curves induced by IgG measured in PBS solutions with different concentrations. With the decrease of PBS concentration, the sensitivity of the IgG sensors gradually increases, and the detection limit is decreased from 10 pM to 100 fM.

To better understand the Debye length effect on the device performance, we calculated the Debye length at different PBS concentrations (Fig. 3C). Here, the total height of antigen-antibody complex is 6.3 ± 1.77 nm. When the ion concentration of PBS is higher than 1 mM, the Debye length is less than the distance between IgG and the gate, and thus, the positive charges on the protein will be screened by anions and cannot form a dipole with the gate. When the concentration of PBS solution is 10 μM or less, the Debye length is increased to more than 22 nm, which is much bigger than the size of the proteins. Therefore, the whole positively charged protein can form a dipole with the gate at this condition, and consequently, the most pronounced effect can be obtained. We can find the lowest detection limit (100 fM) of the IgG sensor when the PBS concentrations are 10 and 1 μM. The relationships between gate voltage shifts and IgG concentrations obtained in 10 and 1 μM PBS solutions are very similar (Fig. 3B), indicating that further increase of the Debye length will not improve the device performance anymore. For the same concentration of IgG while different PBS concentrations used in device characterization (Fig. 3D), we can find that the device responses are also dependent on the PBS concentration. With the decrease of PBS concentration, the shift of the transfer curve increases and saturates at the concentrations around 10 μM.

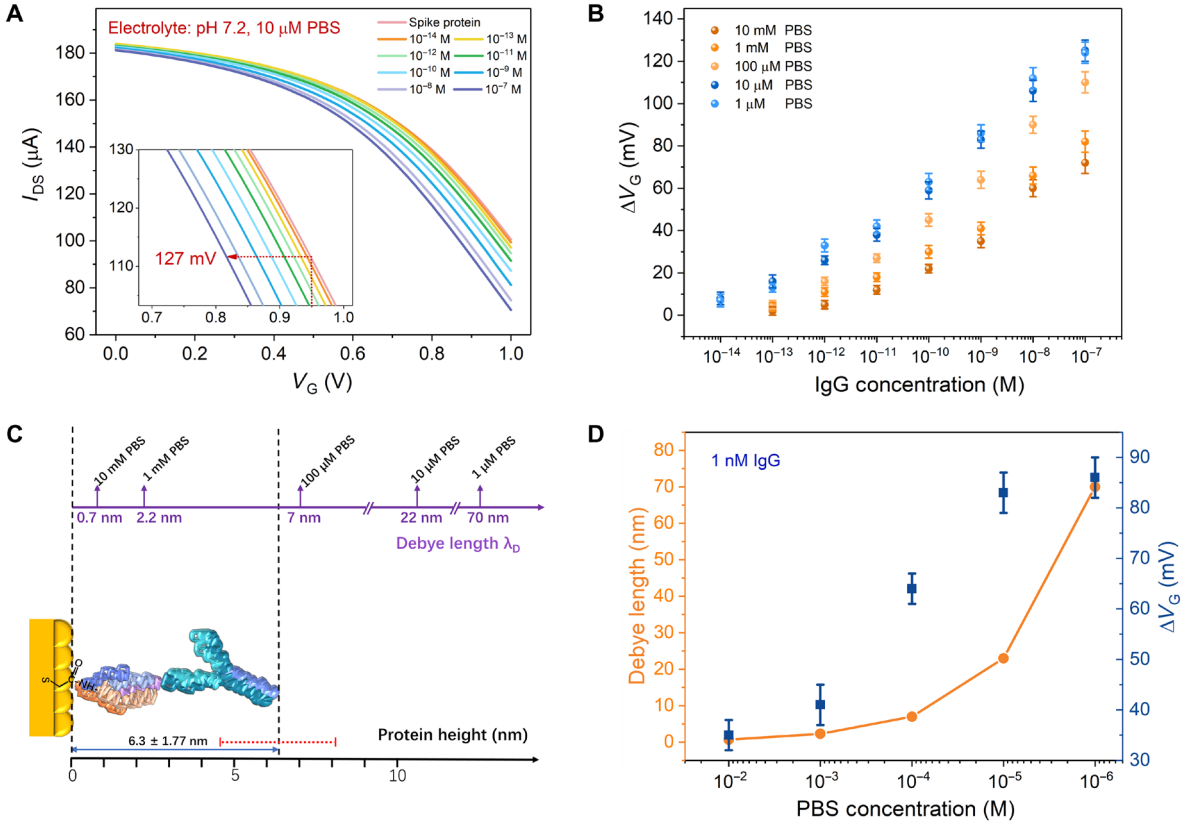


**Fig. 3. Detection of SARS-CoV-2 IgG in diluted PBS solutions.** (**A**) The transfer characteristics of OECTs after incubation of SARS-CoV-2 IgG with different concentrations in sequence (electrolyte: 10 μM PBS, pH 7.2). (**B**) Relative change of the gate voltage $\Delta V_G$ as a function of IgG concentration (electrolyte: PBS with different concentration from 10 mM to 1 μM, pH 7.2). (**C**) The comparation of Debye lengths of PBS solutions and protein height. (**D**) The variation of gate voltage $\Delta V_G$ and Debye length with the change of PBS concentration. The concentration of SARS-CoV-2 IgG solution detected by the device is set to be 1 nM.

## Sensitivity enhancement by increasing net charge of IgG

Another possible approach to improving the sensitivity of the IgG sensor is to increase the surface charge of IgG in solutions. It has been reported that the surface charge of proteins is influenced by the pH value of the solution (*39*). Actually, the surface charge is related to the difference between the pI of the proteins and the pH value of the solution. When pI is identical to the pH value of the solution, no surface charge can be found on the proteins. Considering that SARS-CoV-2 IgG has a pI of 8.2, the protein is more positively charged when it is tested in solutions with lower pH values.

To enhance the surface charge of IgG, the devices were tested in acidic environment with different pH values (from 7.2 to 4.0). When pH value is 5.0, the device response ($\Delta V_G$) to 100 nM SARS-CoV-2 IgG tested in 10 μM electrolyte is increased to 163 mV (Fig. 4A). The device responses to IgG at different pH values are shown in Fig. 4B. Notably, when the pH value of the electrolyte is 5.0, the detection limit is as low as 1 fM. However, the device responses to IgG are decreased when the pH value is further decreased to 4.0. This effect may be related to the weak dissociation of antigen-antibody complex in acidic environment (*40*). In this case, the binding of antigens and antibodies is weakened. Thus, it is reasonable to study the effect of pH between 7.2 and 5.0 on the device performance.

According to site-binding theory, the potential drop Δφ at the interface between protein and the electrolyte is given by (*41*, *42*)

$$\Delta\varphi = 2.3\frac{KT}{q}\alpha\frac{\beta}{\beta+1}(\mathrm{pI}-\mathrm{pH}) \quad (5)$$

where pI is the pH value at the point of zero charge of the protein (pI) and pH is the pH value of the electrolyte. α represents the antibody coverage on the electrode surface, mainly related to the concentration of the protein. β can be expressed by the acidic equilibrium constants of the related amino acids reactions (*41*). Thus, Δφ is the maximum potential drop that can be obtained between the protein and the gate electrode.

As shown in the scheme (Fig. 4C), positively charged antibodies can form an electric dipole on the gate electrode surface. The more net charge the protein carries, the stronger the electric field is created ($E_2 > E_1$; $E_1$ and $E_2$ are the electrostatic fields formed in gate electrolyte interface with pH 7.2 and 5, respectively). Thus, the potential change Δφ increases with the decrease of pH value. The relationship between gate voltage shift and pH value was shown (Fig. 4D). The pH sensitivity is 16 to 26 mV/pH for different IgG concentrations, which are much smaller than the ideal value at room temperature (59 mV/pH) (*42*). This can be attributed to an incomplete protein coverage on the electrode surface. We can find that the pH sensitivity gradually decreases with the decrease of IgG concentration, which further confirms that less coverage of protein can decrease the pH sensitivity. In addition, we have tried to further optimize the concentration of spike protein solution on the gate modification and

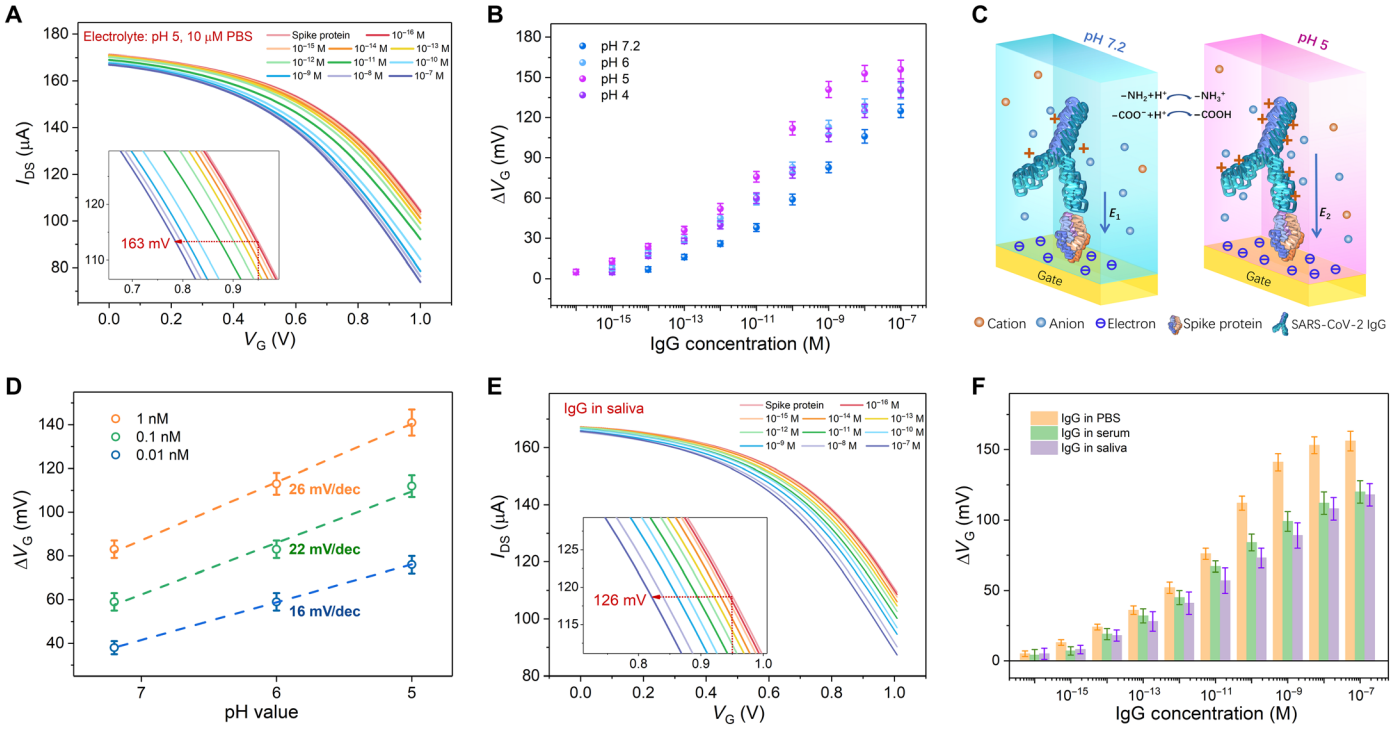


**Fig. 4. Detection of SARS-CoV-2 IgG by measuring OECTs in electrolytes with different pH values.** (**A**) The transfer characteristics of OECTs after incubation of SARS-CoV-2 IgG with different concentrations in sequence (electrolyte: 10 μM PBS, pH 5.0). (**B**) Relative change of the gate voltage $\Delta V_G$ as a function of IgG concentration measured in electrolytes with different pH values. (**C**) The scheme of net charge variation of a protein in electrolytes with different pH values (pH 7.2 and 5.0). (**D**) Relative changes of the gate voltage $\Delta V_G$ for different IgG concentrations (1, 0.1, and 0.01 nM) as a function of pH values of the electrolytes on the OECT. (**E**) The transfer characteristics of OECTs after incubation of SARS-CoV-2 IgG (in saliva) with different concentrations in sequence. (**F**) The comparation of device responds at different IgG concentrations in detecting SARS-CoV-2 IgG in PBS, serum, and saliva (electrolyte: 10 μM PBS, pH 5.0).

found that the device response saturates when the concentration is higher than 0.5 μM. Hence, the gate modification by using 1 μM spike protein solution is the optimum condition (fig. S8).

## SARS-CoV-2 IgG detection in serum and saliva samples

Because the actual detection environment is much more complicated than a PBS solution, we diluted the SARS-CoV-2 IgG in serum and saliva and incubated on gate electrodes for 10 min. After IgG (in diluted saliva) incubation, the transfer curves shift to negative voltage positions (Fig. 4E), which is consistent with the result in PBS solution, while the resultant variations are relatively lower. Figure 4F shows device responses in different detection environments. For 10 fM IgG concentration, the devices show average responds of 19 and 18 mV in serum and saliva samples, respectively, which can meet the requirement of S/N ratio higher than 3. Thus, the detection limits of the devices in measuring IgG in saliva and serum samples are 10 fM. SARS-CoV-2 IgG detections in saliva and serum both show good linear relationship in their concentration range (fig. S9). The detection range in serum is from 10 fM to 100 nM, perfectly matching the serum-specific IgG levels in patients with COVID-19 (*43*). The high sensitivity of the device can also meet the requirement of detecting antibody levels in saliva, which are normally two to four orders of magnitude lower than those in serum (*12*, *13*).

## Enhanced testing speed by voltage pulses

As shown in Fig. 5A, to further reduce the IgG incubation time, voltage pulses (frequency, $10^4$ Hz; voltage, −0.5 V; pulse width, 10 μs; rise/fall time, 5 ns) were applied between the gate and another electrode during incubation. The positively charged IgG molecules can be driven by the electric field to the gate in the solution, and an enhanced antigen and antibody binding efficiency is expected to be achieved (*44*, *45*). The effect of voltage pulses on the binding efficiency of antigens and antibodies was tested under optimized conditions (electrolyte, 10 μM PBS; pH 5; SARA-COV-2 IgG, 100 nM). The device responses ($\Delta V_G$) versus incubation time ($t$) can be fitted with an exponential function $\Delta V_G = A\,[1 - \exp(-t/\tau)]$ (Fig. 5B). With voltage pulses during incubation, the time constant τ is 2.5 min, while the control device without voltage pulse shows the time constant of 4.6 min. Notably, the response of the device can reach 55% after 2-min incubation. For the detection of different concentrations of IgG, the effects of incubation time (with pulse) are shown in Fig. 5C. The transfer characteristics measured at different conditions are presented in fig. S10. Hence, 2-min incubation under voltage pulse can lead to a detection limit of 1 fM in PBS. To ensure that the voltage pulse effect can be applied in practical applications, we added the voltage pulses in the serum and saliva samples. The device responses as a function of incubation time of serum and saliva samples under voltage pulses are shown in fig. S11. The time constant τ was decrease from 5.4 to 3.2 min in serum sample and from 5.3 to 3.5 min in saliva samples, which further indicates that the voltage pulse can accelerate the IgG detection of our devices. In addition, the nonspecific binding from pure serum and saliva is found to be negligible (fig. S11). The relatively longer time constants for the tests in saliva and serum than that in PBS can be attributed to the

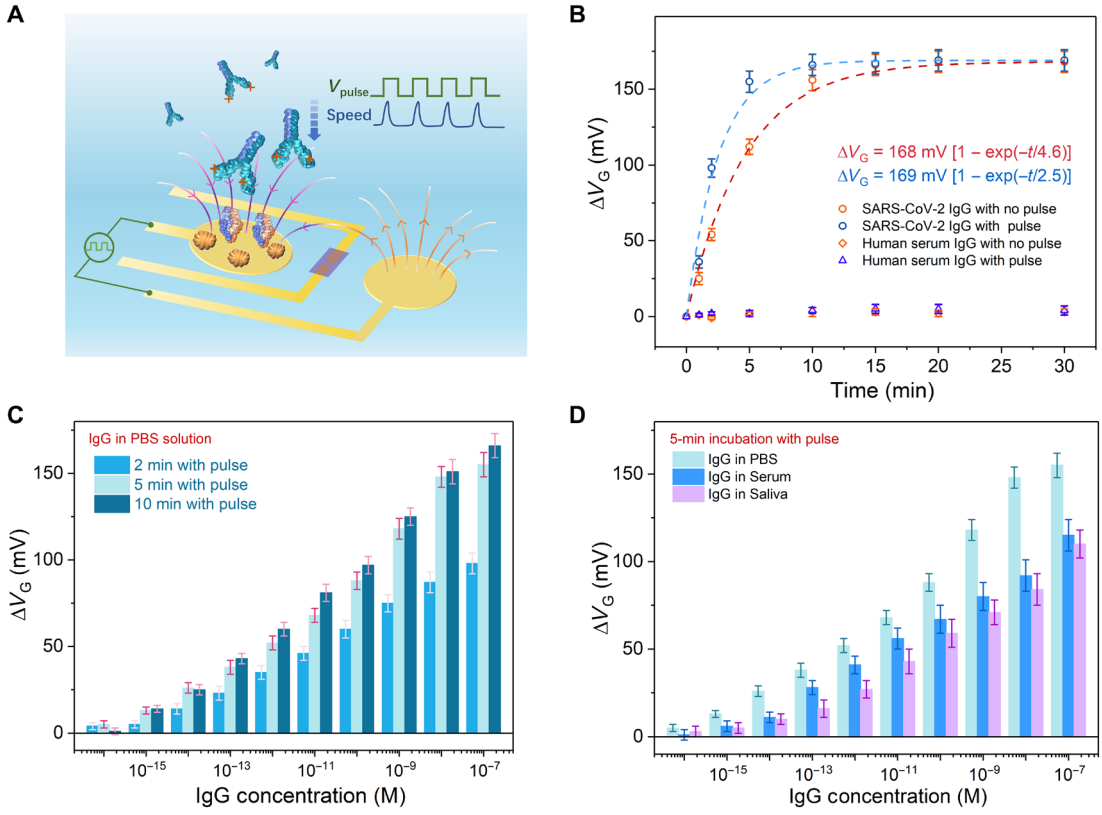


**Fig. 5. Detection of SARS-CoV-2 IgG after applying voltage pulses on gate electrode during IgG incubation.** (**A**) The scheme of IgG migration under voltage pulses between two electrodes during incubation process. (**B**) Relative change of the gate voltage $\Delta V_G$ of OECTs as a function of incubation time (electrolyte: 10 μM PBS, pH 5.0). The control tests were conducted by detecting human serum IgG with the same conditions. (**C**) Relative change of the gate voltage $\Delta V_G$ as a function of IgG concentration in PBS solution with different incubation time. (**D**) Device responses to IgG in PBS, serum, and saliva samples with 5-min incubation under voltage pulses.

complexity and high viscosity of the saliva and serum samples. The device responses at different IgG concentrations of the three type samples were tested with an incubation time of 5 min, and a detection limit of 10 fM IgG can be achieved in saliva and serum samples (Fig. 5D).

## DISCUSSION

In conclusion, we have developed portable, label-free, and low-cost biosensors based on OECTs for rapid and highly sensitive detections of SARS-CoV-2 IgG. The gate electrodes of the OECTs are modified with SARS-CoV-2 spike proteins that can selectively capture the IgG through the specific antibody-antigen reaction. The positively charged IgG molecules in aqueous solutions form electrical dipoles on gate surfaces and modulate the channel currents of the OECTs. By optimizing the measurement conditions, including electrolyte ion concentration and pH value, high device sensitivity has been achieved. The detection limits of the devices can reach 1 fM in aqueous solutions and 10 fM in saliva and serum samples, which are much better than many existing electrochemical methods (see table S1) (*46*–*51*). Notably, the detectable region can cover the concentrations of the specific antibody in the serum and saliva of patients with COVID-19, promising a high potential for practical applications. Faster detection of IgG has been realized by applying voltage pulses on the gates of OECTs during incubation, and stable signal can be obtained within 5 min. The testing process has been remotely operated with a mobile phone by controlling a portable meter via Bluetooth, which can meet the requirement of fast and point-of-care detections of COVID-19 antibody. It is expected that the biosensor can also be used in the fast detections of many other diseases that may generate antibodies.

## MATERIALS AND METHODS

### Materials

Dimethyl sulfoxide (DMSO), glycerin, *N*-(3-(dimethylamino)propyl)–*N*′-ethyl-carbodiimide hydrochloride (EDC), *N*-hydroxysuccinimide (NHS), MAA, BSA, human serum IgG, hydrochloric acid (HCl), ethanolamine (MEA), human serum, and PBS (pH 7.2) solution were all purchased from Sigma-Aldrich Co. SARS-CoV-2 spike protein (S1, His Tag; molecular weight, ~79 kDa) and SARS-CoV-2 IgG (S1 RBD antibody; molecular weight, ~150 kDa) were purchased from GenScript (Nanjing) Co. Ltd. SU-8 photoresists and AZ5214 photoresists were purchased from MicroChemicals GmbH. PEDOT:PSS (Clevios PH-500) aqueous solution was purchased from Heraeus Ltd. GOPS [(3-glycidyloxypropyl)trimethoxysilane] was purchased from International Laboratory, USA.

### Design and fabrication of wireless portable meter

The meter can be divided into three main components (fig. S10), which include microcontroller, OECT-based sensor, and a Bluetooth transmission system. The meter can operate and read data from a

mobile phone via Bluetooth. Details about the design of the portable meter can be found in the Supplementary Materials.

### Device fabrication

The OECT device was fabricated by multilayer photolithography technology. After the first photoetching layer, Au electrode (Cr, 10 nm; Au, 40 nm) was deposited by magnetron sputtering and the liftoff process. The channel length ($L$) and width ($W$) of the devices were 30 and 120 μm, respectively. Through a second layer of photoresist, the SU-8 photoresist was patterned and solidified on the Au electrode, acting as an insulating layer to protect the Au electrodes from the aqueous electrolyte. Last, a channel window was opened by the third layer of photoresist. For preparation of the PEDOT:PSS channel layer, Clevios PH-500 was mixed with DMSO and glycerin (both with a volume ratio of 5%) for improving the conductivity and stability of organic channel. In addition, the cross-linker GOPS was added to the above solution to prohibit PEDOT:PSS dissolution. PEDOT:PSS was then spin-coated on the patterned photoresist and annealed at 110°C for 20 min. Another liftoff process was conducted for removing the redundant PEDOT:PSS film.

### Gate biofunctionalization

To get a clean gate electrode surface, Au electrodes ($D$ = 0.6 mm) were treated with piranha solution ($H_2O_2/H_2SO_4$, v/v = 3/7) for 5 min, followed with regular clean process. The cleaned gold electrode was immersed in the MAA (50 mM) solution in dark overnight to give carboxylic groups, which were activated afterward in a mixed solution of EDC (20 mg/ml) and NHS (10 mg/ml) aqueous solution for 1 hour at 25°C. After immersing the gate electrode in SARS-CoV-2 spike protein solution (1 μM in 10 mM PBS solution, 2 μl) for 2 hours at 25°C, the antigen capturing SAM was formed by conjugation between the amine groups of the antigen and the activated carboxylic groups on the gate surface. Afterward, the gates were treated with MEA (1 M, in 10 mM PBS solution) for 1 hour to eliminate the unreacted carboxylic groups. BSA solution (0.1 mg/ml) was further added for 1 hour to block the remaining nonspecific binding sites of the Au electrode. Last, 5 μl of SARS-CoV-2 IgG with a certain concentration (diluted by PBS/serum/saliva) was added to bind with SARS-CoV-2 spike protein for several minutes at 25°C. During the IgG incubation, voltage pulses were applied to accelerate the antigen antibody binding. After each step of the functionalization, the gate electrodes were rinsed thoroughly in water to remove possible residues.

### Serum and saliva sample preparation

Serum sample was purchased from Sigma-Aldrich, which was from human male AB plasma, U.S. origin, sterile-filtered. Saliva sample was taking from a healthy female volunteer by putting a sterilized cotton ball underside of her tongue for 5 min. The saliva was squeezed from the cotton inside a syringe and injected into a sterile glass bottle. Then, the saliva sample was diluted for five times by 10 mM PBS to decrease the viscosity for further use. For IgG detection in serum and saliva, 1 μM IgG in 10 mM PBS was serially diluted with the serum and saliva samples, respectively.

### Device characterization

The transfer characteristics of the devices were measured by a portable meter that is controlled by a mobile phone through Bluetooth. After each step of the immobilization, the gate electrodes were rinsed thoroughly in water and tested in electrolyte. Transfer characteristics were taken with $V_G$ = 0 to 1 V and $V_{DS}$ = 0.05 V, and the relative change of the gate voltage $\Delta V_G$ was calculated after the antigen-antibody reaction. Electrolytes with different concentrations were obtained by diluting the standard PBS solution with DI water, and HCl was added to adjust the pH value. The voltage pulses (frequency, $10^4$ Hz; voltage, −0.5 V; pulse width, 10 μs; rise/fall time, 5 ns) was generated by a 20-MHz function/arbitrary waveform generator (Agilent, 33220A). The AFM was taken by Scanning Probe Microscope (Bruker NanoScope 8). The FTIR spectroscopy was taken by the Bruker Vertex-70 FTIR. Electrochemical impedance spectroscopy measurements were carried out with a three-electrode system using a Zahner Zennium pro electrochemical workstation, with platinum gauze counter electrode and Ag/AgCl reference electrode. The electrolyte is 10 mM PBS (pH 7.2).

## SUPPLEMENTARY MATERIALS

Supplementary material for this article is available at https://science.org/doi/10.1126/sciadv.abg8387

View/request a protocol for this paper from *Bio-protocol*.

## REFERENCES AND NOTES


1. P. Yang, X. Wang, COVID-19: A new challenge for human beings. *Cell. Mol. Immunol.* **17**, 555–557 (2020).
2. X. Li, M. Geng, Y. Peng, L. Meng, S. Lu, Molecular immune pathogenesis and diagnosis of COVID-19. *J. Pharm. Anal.* **10**, 102–108 (2020).
3. A. Petherick, Developing antibody tests for SARS-CoV-2. *Lancet* **395**, 1101–1102 (2020).
4. B. Böger, M. M. Fachi, R. O. Vilhena, A. de Fátima Cobre, F. S. Tonin, R. Pontarolo, Systematic review with meta-analysis of the accuracy of diagnostic tests for COVID-19. *Am. J. Infect. Control* **49**, 21–29 (2021).
5. S. Assadiasl, Y. Fatahi, M. Zavvar, M. H. Nicknam, COVID-19: Significance of antibodies. *Hum. Antibodies* **28**, 287–297 (2020).
6. K. Li, B. Huang, M. Wu, A. Zhong, L. Li, Y. Cai, Z. Wang, L. Wu, M. Zhu, J. Li, Z. Wang, W. Wu, W. Li, B. Bosco, Z. Gan, Q. Qiao, J. Wu, Q. Wang, S. Wang, X. Xia, Dynamic changes in anti-SARS-CoV-2 antibodies during SARS-CoV-2 infection and recovery from COVID-19. *Nat. Commun.* **11**, 6044 (2020).
7. A. E. Muruato, C. R. Fontes-Garfias, P. Ren, M. A. Garcia-Blanco, V. D. Menachery, X. Xie, P. Y. Shi, A high-throughput neutralizing antibody assay for COVID-19 diagnosis and vaccine evaluation. *Nat. Commun.* **11**, 4059 (2020).
8. I. Eckerle, B. Meyer, SARS-CoV-2 seroprevalence in COVID-19 hotspots. *Lancet* **396**, 514–515 (2020).
9. R. W. Peeling, C. J. Wedderburn, P. J. Garcia, D. Boeras, N. Fongwen, J. Nkengasong, A. Sall, A. Tanuri, D. L. Heymann, Serology testing in the COVID-19 pandemic response. *Lancet Infect. Dis.* **20**, e245–e249 (2020).
10. Q. Wang, Q. Du, B. Guo, D. Mu, X. Lu, Q. Ma, Y. Guo, L. Fang, B. Zhang, G. Zhang, X. Guo, A method to prevent SARS-CoV-2 IgM false positives in gold immunochromatography and enzyme-linked immunosorbent assays. *J. Clin. Microbiol.* **58**, e00375 (2020).
11. I. Montesinos, D. Gruson, B. Kabamba, H. Dahma, S. Van den Wijngaert, S. Reza, V. Carbone, O. Vandenberg, B. Gulbis, F. Wolff, H. Rodriguez-Villalobos, Evaluation of two automated and three rapid lateral flow immunoassays for the detection of anti-SARS-CoV-2 antibodies. *J. Clin. Virol.* **128**, 104413 (2020).
12. T. Liu, J. Hsiung, S. Zhao, J. Kost, D. Sreedhar, C. V. Hanson, K. Olson, D. Keare, S. T. Chang, K. P. Bliden, P. A. Gurbel, U. S. Tantry, J. Roche, C. Press, J. Boggs, J. P. Rodriguez-Soto, J. G. Montoya, M. Tang, H. Dai, Quantification of antibody avidities and accurate detection of SARS-CoV-2 antibodies in serum and saliva on plasmonic substrates. *Nat. Biomed. Eng.* **4**, 1188–1196 (2020).
13. X. Li, C. Pomares, F. Peyron, C. J. Press, R. Ramirez, G. Geraldine, I. Cannavo, E. Chapey, P. Levigne, M. Wallon, J. G. Montoya, H. Dai, Plasmonic gold chips for the diagnosis of *Toxoplasma gondii*, CMV, and rubella infections using saliva with serum detection precision. *Eur. J. Clin. Microbiol. Infect. Dis.* **38**, 883–890 (2019).
14. B. Isho, K. T. Abe, M. Zuo, A. J. Jamal, B. Rathod, J. H. Wang, Z. Li, G. Chao, O. L. Rojas, Y. M. Bang, A. Pu, N. Christie-Holmes, C. Gervais, D. Ceccarelli, P. Samavarchi-Tehrani, F. Guvenc, P. Budylowski, A. Li, A. Paterson, F. Y. Yue, L. M. Marin, L. Caldwell, J. L. Wrana, K. Colwill, F. Sicheri, S. Mubareka, S. D. Gray-Owen, S. J. Drews, W. L. Siqueira, M. Barrios-Rodiles, M. Ostrowski, J. M. Rini, Y. Durocher, A. J. McGeer, J. L. Gommerman, A.-C. Gingras, Persistence of serum and saliva antibody responses to SARS-CoV-2 spike antigens in COVID-19 patients. *Sci. Immunol.* **5**, eabe5511 (2020).

15. J. Rivnay, S. Inal, A. Salleo, R. M. Owens, M. Berggren, G. G. Malliaras, Organic electrochemical transistors. *Nat. Rev. Mater.* **3**, 17086 (2018).
16. E. Macchia, K. Manoli, B. Holzer, C. Di Franco, M. Ghittorelli, F. Torricelli, D. Alberga, G. F. Mangiatordi, G. Palazzo, G. Scamarcio, L. Torsi, Single-molecule detection with a millimetre-sized transistor. *Nat. Commun.* **9**, 3223 (2018).
17. P. Romele, P. Gkoupidenis, D. A. Koutsouras, K. Lieberth, Z. M. Kovacs-Vajna, P. W. M. Blom, F. Torricelli, Multiscale real time and high sensitivity ion detection with complementary organic electrochemical transistors amplifier. *Nat. Commun.* **11**, 3743 (2020).
18. P. Lin, F. Yan, Organic thin-film transistors for chemical and biological sensing. *Adv. Mater.* **24**, 34–51 (2012).
19. P. Lin, X. Luo, I. M. Hsing, F. Yan, Organic electrochemical transistors integrated in flexible microfluidic systems and used for label-free DNA sensing. *Adv. Mater.* **23**, 4035–4040 (2011).
20. P. Lin, F. Yan, J. Yu, H. L. Chan, M. Yang, The application of organic electrochemical transistors in cell-based biosensors. *Adv. Mater.* **22**, 3655–3660 (2010).
21. Y. Fu, N. Wang, A. Yang, H. K. Law, L. Li, F. Yan, Highly sensitive detection of protein biomarkers with organic electrochemical transistors. *Adv. Mater.* **29**, 1703787 (2017).
22. A. Yang, Y. Li, C. Yang, Y. Fu, N. Wang, L. Li, F. Yan, Fabric organic electrochemical transistors for biosensors. *Adv. Mater.* **30**, e1800051 (2018).
23. N. Wang, Y. Liu, Y. Fu, F. Yan, AC measurements using organic electrochemical transistors for accurate sensing. *ACS Appl. Mater. Interfaces* **10**, 25834–25840 (2018).
24. T. Burgi, Properties of the gold-sulphur interface: From self-assembled monolayers to clusters. *Nanoscale* **7**, 15553–15567 (2015).
25. Z. L. Gao, P. Ducos, H. C. Ye, J. Zauberman, A. Sriram, X. P. Yang, Z. Y. Wang, M. W. Mitchell, D. Lekkas, D. Brisson, A. T. C. Johnson, Graphene transistor arrays functionalized with genetically engineered antibody fragments for Lyme disease diagnosis. *2D Mater.* **7**, 024001 (2020).
26. V. Ierardi, F. Ferrera, E. Millo, G. Damonte, G. Filaci, U. Valbusa, Bioactive surfaces for antibody-antigen complex detection by atomic force microscopy. *J. Phys. Conf. Ser.* **439**, 012001 (2013).
27. P. I. Haris, F. Severcan, FTIR spectroscopic characterization of protein structure in aqueous and non-aqueous media. *J. Mol. Catal. B: Enzym.* **7**, 207–221 (1999).
28. J. Kong, S. Yu, Fourier transform infrared spectroscopic analysis of protein secondary structures. *Acta Biochim. Biophys. Sin.* **39**, 549–559 (2007).
29. G. L. Long, J. D. Winefordner, Limit of detection. A closer look at the IUPAC definition. *Anal. Chem.* **55**, 712A–724A (1983).
30. I. Gitlin, J. D. Carbeck, G. M. Whitesides, Why are proteins charged? Networks of charge-charge interactions in proteins measured by charge ladders and capillary electrophoresis. *Angew. Chem. Int. Ed.* **45**, 3022–3060 (2006).
31. D. A. Bernards, G. G. Malliaras, Steady-state and transient behavior of organic electrochemical transistors. *Adv. Funct. Mater.* **17**, 3538–3544 (2007).
32. S. Inal, G. G. Malliaras, J. Rivnay, Benchmarking organic mixed conductors for transistors. *Nat. Commun.* **8**, 1767 (2017).
33. D. A. Bernards, D. J. Macaya, M. Nikolou, J. A. DeFranco, S. Takamatsu, G. G. Malliaras, Enzymatic sensing with organic electrochemical transistors. *J. Mater. Chem.* **18**, 116–120 (2008).
34. M. Thompson, L. E. Cheran, M. Zhang, M. Chacko, H. Huo, S. Sadeghi, Label-free detection of nucleic acid and protein microarrays by scanning Kelvin nanoprobe. *Biosens. Bioelectron.* **20**, 1471–1481 (2005).
35. P. Kukic, D. Farrell, L. P. McIntosh, E. B. García-Moreno, K. S. Jensen, Z. Toleikis, K. Teilum, J. E. Nielsen, Protein dielectric constants determined from NMR chemical shift perturbations. *J. Am. Chem. Soc.* **135**, 16968–16976 (2013).
36. N. Bhalla, Y. Pan, Z. Yang, A. F. Payam, Opportunities and challenges for biosensors and nanoscale analytical tools for pandemics: COVID-19. *ACS Nano* **14**, 7783–7807 (2020).
37. E. Stern, R. Wagner, F. J. Sigworth, R. Breaker, T. M. Fahmy, M. A. Reed, Importance of the Debye screening length on nanowire field effect transistor sensors. *Nano Lett.* **7**, 3405–3409 (2007).
38. M. L. Hammock, O. Knopfmacher, B. D. Naab, J. B.-H. Tok, Z. A. Bao, Investigation of protein detection parameters using nanofunctionalized organic field-effect transistors. *ACS Nano* **7**, 3970–3980 (2013).
39. R. A. Hartvig, M. van de Weert, J. Ostergaard, L. Jorgensen, H. Jensen, Protein adsorption at charged surfaces: The role of electrostatic interactions and interfacial charge regulation. *Langmuir* **27**, 2634–2643 (2011).
40. Q. Li, M. Gordon, C. Cao, K. E. Ugen, D. Morgan, Improvement of a low pH antigen-antibody dissociation procedure for ELISA measurement of circulating anti-Aβ antibodies. *BMC Neurosci.* **8**, 22 (2007).
41. P. Bergveld, Thirty years of ISFETOLOGY: What happened in the past 30 years and what may happen in the next 30 years. *Sens. Actuators B* **88**, 1–20 (2003).
42. F. Yan, P. Estrela, Y. Mo, P. Migliorato, H. Maeda, S. Inoue, T. Shimoda, Polycrystalline silicon ion sensitive field effect transistors. *Appl. Phys. Lett.* **86**, 053901 (2005).
43. W. Zeng, H. Ma, C. Ding, Y. Yang, Y. Sun, X. Huang, W. He, Y. Xiang, Y. Gao, T. Jin, Characterization of SARS-CoV-2-specific antibodies in COVID-19 patients reveals highly potent neutralizing IgA. *Signal Transduct. Target. Ther.* **6**, 35 (2021).
44. S. Emaminejad, M. Javanmard, C. Gupta, S. Chang, R. W. Davis, R. T. Howe, Tunable control of antibody immobilization using electric field. *Proc. Natl. Acad. Sci. U.S.A.* **112**, 1995–1999 (2015).
45. D. R. Hekstra, K. I. White, M. A. Socolich, R. W. Henning, V. Srajer, R. Ranganathan, Electric-field-stimulated protein mechanics. *Nature* **540**, 400–405 (2016).
46. R. M. Torrente-Rodríguez, H. Lukas, J. Tu, J. Min, Y. Yang, C. Xu, H. B. Rossiter, W. Gao, SARS-CoV-2 RapidPlex: A graphene-based multiplexed telemedicine platform for rapid and low-cost COVID-19 diagnosis and monitoring. *Matter* **3**, 1981–1998 (2020).
47. R. Funari, K. Y. Chu, A. Q. Shen, Detection of antibodies against SARS-CoV-2 spike protein by gold nanospikes in an opto-microfluidic chip. *Biosens. Bioelectron.* **169**, 112578 (2020).
48. X. Tan, M. Krel, E. Dolgov, S. Park, X. Li, W. Wu, Y. L. Sun, J. Zhang, M. K. Khaing Oo, D. S. Perlin, X. Fan, Rapid and quantitative detection of SARS-CoV-2 specific IgG for convalescent serum evaluation. *Biosens. Bioelectron.* **169**, 112572 (2020).
49. Z. Wang, Z. Zheng, H. Hu, Q. Zhou, W. Liu, X. Li, Z. Liu, Y. Wang, Y. Ma, A point-of-care selenium nanoparticle-based test for the combined detection of anti-SARS-CoV-2 IgM and IgG in human serum and blood. *Lab Chip* **20**, 4255–4261 (2020).
50. Q. Lin, D. Wen, J. Wu, L. Liu, W. Wu, X. Fang, J. Kong, Microfluidic immunoassays for sensitive and simultaneous detection of IgG/IgM/antigen of SARS-CoV-2 within 15 min. *Anal. Chem.* **92**, 9454–9458 (2020).
51. Z. Li, Y. Yi, X. Luo, N. Xiong, Y. Liu, S. Li, R. Sun, Y. Wang, B. Hu, W. Chen, Y. Zhang, J. Wang, B. Huang, Y. Lin, J. Yang, W. Cai, X. Wang, J. Cheng, Z. Chen, K. Sun, W. Pan, Z. Zhan, L. Chen, F. Ye, Development and clinical application of a rapid IgM-IgG combined antibody test for SARS-CoV-2 infection diagnosis. *J. Med. Virol.* **92**, 1518–1524 (2020).



**Acknowledgments**

**Funding:** This work is financially supported by the Research Grants Council (RGC) of Hong Kong, China (project no. C5015-15G) and by the Innovation and Technology Commission of Hong Kong (project no. MRP/040/18X). **Author contributions:** F.Y. conceived the experiments. H.L. carried most experiments and data analysis. A.Y., P.L., and Y.L. design and fabricated the portable meter and OECT device. J.S. and N.W. assisted in device characterization. H.K.-w.L. has contributed to the serum and saliva test. The manuscript was written by F.Y. and H.L. All authors contributed to manuscript review, revision, and finalization. **Competing interests:** The authors declare that they have no competing interests. **Data and materials availability:** All data needed to evaluate the conclusions in the paper are present in the paper and/or the Supplementary Materials.

Submitted 30 January 2021
Accepted 26 July 2021
Published 15 September 2021
10.1126/sciadv.abg8387

**Citation:** H. Liu, A. Yang, J. Song, N. Wang, P. Lam, Y. Li, H. K.-w. Law, F. Yan, Ultrafast, sensitive, and portable detection of COVID-19 IgG using flexible organic electrochemical transistors. *Sci. Adv.* **7**, eabg8387 (2021).

ScienceAdvances

# Ultrafast, sensitive, and portable detection of COVID-19 IgG using flexible organic electrochemical transistors

Hong LiuAnneng YangJiajun SongNaixiang WangPuiyiu LamYuenling LiHelen Ka-wai LawFeng Yan

*Sci. Adv.*, 7 (38), eabg8387. • DOI: 10.1126/sciadv.abg8387







*Science Advances* (ISSN ) is published by the American Association for the Advancement of Science. 1200 New York Avenue NW, Washington, DC 20005. The title *Science Advances* is a registered trademark of AAAS.